Building and Environment 248 (2024) 111078

Contents lists available at ScienceDirect

Building and Environment

journal homepage: www.elsevier.com/locate/buildenv

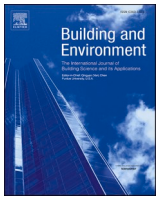

# Occupants' interaction with building services: Development of a camera-based method for detailed monitoring of windows, shadings, and lights

Julian Donges [a,*], Federica Morandi [a], Alessandro Prada [b], Francesca Cappelletti [c], Andrea Gasparella [a]

[a] Free University of Bozen-Bolzano, Faculty of Engineering, Bolzano, Italy
[b] University of Trento, Dept. of Civil Environmental and Mechanical Engineering, Trento, Italy
[c] IUAV University of Venice, Dept. of Architecture and Arts, Venice, Italy

ARTICLE INFO

*Keywords:*
Behavioral monitoring
Object identification
Image processing
Window operation
Indoor environmental quality
Natural ventilation

ABSTRACT

Several energy gains or losses in buildings are influenced by occupant interactions with building services, such as lighting or HVAC systems, thermostat settings, and window and shading operations. Occupant behavior is usually triggered by discomfort, nevertheless actions taken to restore comfort can have an impact on final energy demand. Thus, an accurate energy assessment for both new and retrofit building design must properly account for occupant behavior, based on reliable models developed from real case studies and detailed monitoring. This work presents a new approach for continuous and non-intrusive monitoring of window opening angle, shading position, and lighting operation to determine the net air exchange area for ventilation. A camera-based device and a post-processing algorithm are developed, and a monitoring campaign over 6 month is carried out to showcase the monitoring system. The device consists of a camera setup connected to a microprocessor, and a dedicated script which enables the device to track window opening, shading movement and lighting operation through target and object identification. Results of the prototyping case study show that the proposed system can effectively detect window opening angles and shutter positions, dealing with multiple windows and shutters simultaneously and allowing the deployment of the benefits of continuous monitoring. The explored application is the direct use of the collected data for the calculation of natural ventilation rates from the net exchange area (EN 16798-7) over long term datasets. As future development, the monitoring system will be used to develop accurate behavioral models based on the experimental data to analyze and suggest the occupant's response to discomfortable conditions in order to improve indoor air quality and save energy.

## 1. Introduction

As society moves towards a reduction of greenhouse gas emissions in the building sector, designers need to push beyond cost-optimality criteria and move towards nZEB targets while improving indoor comfort and well-being for occupants. When approaching these targets, building air infiltration and natural ventilation become major elements in the buildings' thermal balance and need to be carefully considered to ensure efficient use of energy while maintaining appropriate indoor environmental quality. Therefore, for naturally ventilated buildings relying on manual window operation, an in-depth understanding of the occupants' related behavioral patterns is key.

In Italy and most European countries, the building stock relies heavily on natural ventilation [1]. Highly occupied spaces, where many people gather for prolonged periods, often suffer from poor air quality, with elevated concentrations of $CO_2$ and air pollutants that need to be controlled. Monitoring campaigns have shown that some educational spaces cannot maintain Indoor Air Quality (IAQ), ensuring $CO_2$ concentration below 800 ppm for more than 60% of the time [2]. Therefore, natural ventilation as the main strategy and indicator for IAQ and thermal comfort still needs further investigation to collect data, assess its limitations, understand triggers causing occupants to take action, evaluate the interactions with building services and components, and develop behavioral models to improve building performance simulation

* Corresponding author.
*E-mail address:* julian.donges@natec.unibz.it (J. Donges).

https://doi.org/10.1016/j.buildenv.2023.111078
Received 22 August 2023; Received in revised form 21 November 2023; Accepted 27 November 2023
Available online 30 November 2023

[3,4]. Ventilation gained relevance during the Covid-19 pandemic which requested an increased control of air quality. Few studies had investigated in schools [5–7], while most studies reviewed ventilation behaviors and strategies in office buildings ([8–13]; A. [14,15]) and residential buildings [10,16–19]. Ventilation is a fundamental factor in indoor environmental quality (IEQ) and building performance, influencing occupant comfort, health, and energy efficiency. The COVID-19 pandemic, moreover, heightened awareness of ventilation's role in mitigating disease transmission within indoor spaces and underscored its critical importance in addressing public health concerns in built environments. This study therefore aims to contribute to this new awareness by understanding and quantifying ventilation in buildings.

The International Energy Agency has defined occupant behavior as a key driver of building energy performance. Buildings are sensitive to human interactions, especially with regard to energy usage [20]. Behavioral responses can be triggered by various drivers, such as physiological, psychological, social or contextual factors, most of which are difficult to identify or quantify [21]. Therefore, studies focusing on behavioral monitoring and prediction are crucial for assessing the related impact on indoor environmental quality and the energy use, and more in detail for the development of optimized ventilation strategies [22]. In many works, window operation appears the most common and preferred behavior [19]. It is found to have a great impact not only on IAQ, but on thermal comfort, and noise as well. The interaction between occupants and the building envelope is crucial in naturally-ventilated buildings, as such buildings are often characterized by insufficient air exchange rates [23]. In addition, natural ventilation is under the spotlight for promoting other sources of discomfort such as drafts discomfort and cross-contamination between rooms in the case of viral loads [24].

Common approaches to model natural ventilation in energy and comfort assessments are still not very reliable and often contribute to a difference between predicted and measured performance. This contributes to the so-called performance gap [25], namely the difference between the predicted performance of a building and its actual performance under post-occupancy conditions, which according to some references is mostly caused by human behavior as an influencing factor [22]. If this is the case, accurate building energy simulation for both new and retrofit building designs must correctly represent human behavior.

Modeling natural ventilation for energy and comfort assessments is a complex task due to multiple challenges. Common approaches often lack reliability due to the intricate nature of natural ventilation, influenced by factors such as outdoor conditions, dynamic airflow patterns, and occupant behavior. There are models relying on CFD [26], which would serve for increased accuracy if needed for the research scope. However, CFD models are computationally time-consuming and harder to use for annual simulations. The non-linear and dynamic airflow in naturally ventilated spaces, as well as unexpected variables like sudden weather changes, further complicate predictions. However, also the multifaceted and variable nature of occupant behavior plays a significant role in influencing airflow rates. Given these complexities, the reliability of traditional models is often limited, highlighting the need for advanced monitoring and predictive methods. Hyun et al. [26] explores these sources of uncertainty in models for natural ventilation estimation in the context of tall buildings, underscoring the significance of the net exchange area as the second most influential parameter in the model, following wind speed.

Accurate and detailed data on case studies are needed to develop and refine reliable behavioral models [17,27]. However, common approaches to monitor occupant behavior, especially with respect to window opening, often provide only binary information about the window state (i.e., open/closed). Information on the window opening angle is relevant to properly estimate the net exchange area [28]. For example, to estimate ventilation rates, the European standard EN 16798-7:2018 [29] outlines an approach based on the window opening angle and shading factor. The amount of airflow through a window depends on the window open area, in addition to wind speed and direction, turbulence conditions, and the indoor-outdoor temperature difference [30]. The window open area is given by the product of the window size and the opening fraction, which for casement or tilt and turn windows can be calculated using the opening angle and the shading positions. It is essential to acknowledge that diverse shading types, including interior and exterior shadings made of different materials, can exert varying degrees of influence on ventilation. This variation is often characterized by the discharge coefficient (Cd) used in building simulations, which signifies the resistance the shading imposes to airflow. Cd accounts for the ability of a shading system to facilitate or restrict the flow of outdoor air into the indoor space [31]. These values play an important role in calculating the changes in the magnitude of the net exchange area with increasing window opening angle and obstacles such as shadings covering a portion of the opening but still are difficult to monitor in case studies. In conclusion, a detailed monitoring approach of both – the window opening angle and the shading position – is essential to properly estimate the ventilation rate.

### 1.1. Approaches for monitoring window opening behavior

Typical approaches to predict occupant interactions with windows and shadings rely on binary or discrete probabilistic prediction of opening angles and shading positions [17,32,33]. These models are typically calibrated and validated using experimental data collected with accelerometers [34], contact sensors [19], air speed measurements [35], Bluetooth devices [36], ultrasound [37], or laser sensors [38]. A detailed comparison of the commonly used approaches is found in Donges et al. [39].

More and more applications rely on cameras to automatically monitor behavior. Camera-based applications included (i) occupancy counting to improve management and control of ambient light, airflow, and temperature as described in Alishahi et al. [40], (ii) average window luminance and background luminance measurements [13] and (iii) forehead temperature measurements using thermal imaging cameras to estimate human comfort [41]. Camera based devices have been introduced for luminance mapping and glare control (M. [42]; M. [43]), or mapping heat dissipation on monitored surfaces [44], and similar purposes. A camera-based system can be used to extract the window opening information through appropriate image post-processing. The resolution levels achieved by camera-based approaches are much finer than the above measurement methods and are only limited by the sensor resolution. Recent studies have dealt with the development of camera-based tools to detect window operation from the outside [45,46]. Some research proposed using the devices to monitor entire facades and determine three discrete states of the window: closed, partially open, and fully open [47]. Other studies used similar approaches to identify façade features like texture and shape, in the context of advancing the capabilities of 3D cityscape modeling using aerial and ground-based imagery [48].

While monitoring from the outside may include information about an entire facade, indoor applications reduce the information obtained to a single space (usually a single facade in a single room), providing valuable information even if limited to the space where the experiment or monitoring campaign is conducted. To the authors' knowledge, only a few studies have addressed the indoor application of a camera to monitor building services [45,49].

Almost all mentioned non-camera-based devices have two drawbacks: (i) they provide binary outputs or (ii) they have possible information losses due to limited working distance, viewing angle or spatial resolution. Therefore, for simplicity, most research considers only the binary state of building services such as lights, windows, and shadings. The use of binary output leads to an overestimation of the influence of windows on the ventilation rate. While camera-based approaches overcome these drawbacks by increasing the resolution of window movement or position, only few studies [45,49] within the literature considered the measurement of window opening angles.

Given the potential benefits of a camera-based solution (such as reduced wiring, high measurement resolution, and ease of application), the research presented here focuses on this monitoring approach and the corresponding image post-processing to extract the necessary information.

### 1.2. Postprocessing approaches for camera images

The key component to monitor occupant behavior using a camera is the post-processing of the obtained images. Image processing is used to get the information contained in an image and enables us to automate the process of data extraction. The main idea of the post-processing algorithm is to detect the position or state of predefined targets, objects, or similarities in image patterns found in training data. There are two main families in image post-processing identified in the literature, based on (i) the use of Artificial Intelligence (AI) using deep learning frameworks such as Convolutional Neural Networks (CNNs), or (ii) post-processing using object identification, which can be edge detection, geometrical targets, or colored targets.

#### 1.2.1. The use of AI

With the growth of image-based deep learning strategies for various applications, the use of cameras to extract valuable information has gained new interest. In recent literature, Convolutional Neural Networks (CNNs) and similar vision-based deep learning frameworks have been used to post-process images and automate information extraction from acquired datasets. CNNs are part of the larger field of artificial intelligence. Rather than following explicitly programmed instructions – as it would be the case for object identification - CNNs allow computers to train on previously prepared ground-truth datasets and use decision classifications to extract the required information. Deep learning opens up a vast field for developing post-processing algorithms that are calibrated using previously acquired training data. The training data should be proven to be true (ground truth data) to reliably train the algorithm for the specific problem (K. W. [50]). Next to the images themselves, the corresponding value of the monitored building service - e.g., an angle of 0–90° for windows, the exact position of shades, or 0/1 state for lights - is provided within the training data [45]. CNN algorithms become efficient once adequately trained, which is the most time-consuming and resource-intensive phase, especially when the dataset includes over 10, 000+ images taken in defined states of the façade [46]. The training time depends on factors like model complexity and hardware, while the characteristics of the training images (building/room/façade) vary depending on the project's scope but can potentially be adapted to similar environments. Therefore, CNN is more suitable for long-term, ongoing monitoring, which outweighs the preparation effort for the training dataset. In the literature, some studies apply cameras to the entire façade and use CNNs to automatically detect the state of windows [47,49].

#### 1.2.2. Object identification

An approach that provides more control over the individual processing steps is object identification. It allows an easy-to-use approach [49] without the need for extensive training datasets, which is more suitable for short-term monitoring. It includes perspective adjustment, grayscale conversion or color filtering, edge detection, and image segmentation. Object identification is a powerful tool used to detect recurring patterns in an image, such as the position of an edge or of a target defined by its orientation, size, and thickness. Applied to windows, it allows to monitor the position of the window's frame [49]. A preliminary work by the authors [39] raised concerns about the reliability of the edge detection algorithms, since the edges of shades and window frames may overlap when multiple targets are monitored. Alternatively, the geometric shape of objects, such as circular or rectangular targets, can be detected, leading to the possibility of mounting geometric targets on building services. Preliminary studies have shown that round objects are often found throughout the image due to blur or light rays that cause circular reflections, making the choice of the shape of the target a crucial aspect. Finally, recognition of color code values can similarly be used or complemented to find targets in an image, with increased reliability if unique colors are used [51]. A previous work of the authors [39] highlighted the limitations regarding the use of RGB values which require calibration for various illumination categories. Therefore, automatic brightness adjustment and white balancing of an image can increase the reliability of color recognition. With the use of different color spaces which are more suitable for color categorization like HSV (Hue, Saturation, Value) or HSL (Hue, Saturation, Lightness) this problem is overcome [52]. The RGB vectors can be projected and converted to this more suitable representation. While the RGB color model refers to the biological processing of colors in the human visual system, the HSV color model corresponds to the human perception of color similarity (Valín & Alberto J. V., 2019). The results of transforming a test series of images into the HSV color space are briefly presented in Section 3.

### 1.3. Research gap and scope of study

The literature review indicates that knowledge of the opening angle of windows and shading positions are fundamental to ensure accurate estimation of ventilation rates and related energy losses and comfort assessments. Since windows and shades are typically operated in a non-binary manner, an approach is needed that provides continuous monitoring along their movement path. At the same time, current building monitoring approaches often provide binary information due to the limited resolution used by conventional sensors to monitor window opening as described in Section 1.1. Only very few works focus on a continuous measurement of building services ([30] & Wong et al., 2023), whereas none of the analyzed literature provided an approach to simultaneously monitor shading position and window angle which is fundamental for a detailed analysis of the ventilation rate. This research gap is tried to be overcome by the proposed work. A promising approach is presented which foresees the use of cameras due to their wide range of applications and fine sensor resolution. Image-based monitoring requires appropriate image processing. CNNs seem to be a promising approach to automate image processing using large training data sets [46]. However, the development of large training datasets is time-intensive and therefore more suitable for long-term monitoring campaigns or stationary sensors. Avoiding the preparation of time-consuming training datasets without reducing the value of the information gained to binary states is an approach that, to the authors' knowledge, has not yet been fully explored.

Therefore, the scope of this study is to develop and demonstrate the effectiveness and ease of use of a new monitoring instrumentation to provide continuous and non-intrusive monitoring of the window opening angle, shading position, with the additional possibility of recording artificial lighting operation, using a straightforward post-processing approach without the need for large training data sets. One of the advantages of this approach is its applicability to both short-term and long-term monitoring campaigns, in some cases as a preparatory step for the application of CNN based approaches, highlighting the relevance of continuous monitoring in detail. Consequently, the focus of the proposed approach is on camera-based monitoring from the inside of a room, aiming to be used in the future as a ready-to-use instrument for monitoring behavioral patterns providing further insights into IAQ and energy efficiency.

## 2. Methodology

The methodology focuses on the development of both the hardware and the post-processing algorithm to enable examination of aspects of occupant behavior such as window opening angles, shading positions, as well as lighting.

As reported, opening angles and shading position are key to assess the open fraction of the window area and determine the effectiveness of natural ventilation. The fraction of the air exchange area from its maximum considering a simple European style casement window is shown in Fig. 1 where the red areas $A_1$ and $A_2$ represent the air exchange area. Assuming an operation in turn mode, where the window is rotated around its hinge along the vertical axis, opening angles around 20° already represent an opening fraction of about 50% whereas already at 40° the maximum air exchange is achieved. For detailed analysis and in-depth understanding, small opening angles, which cannot be represented as binary information, play an important role and significantly affect the real and calculated air flow.

This section illustrates the experimental setup and evaluation algorithm. It consists of three parts: (i) the description of the chosen hardware components for the monitoring device, (ii) the development of a reliable post-processing algorithm to analyze the images, and (iii) the determination of accuracy constraints of the device and a proof of concept using real field test data and boundary conditions obtained during a 6-month pilot case study.

### 2.1. Hardware components

This section identifies and briefly introduces the major hardware components to provide a better understanding of the early design phase of the device.

#### 2.1.1. Microcomputer and camera

A microcomputer is used for automated data acquisition and as a handling unit for post-processing, storage and remote access. Among the solutions available on the market, a Raspberry Pi 4B with 8 GB Ram is chosen from a range of possibilities evaluated in Donges et al. [39]. The strong points of the setup are its Wi-Fi connectivity for data extraction, compactness, and the possibility for autonomous operation as well as remote maintenance and data download. Moreover, it allows the installation of additional sensors and instruments, if desired. A camera - to monitor windows, shades, and lights - and a switch - to monitor door movement - are connected to the Raspberry's GPIO board. The key components for image acquisition are the image sensor and the camera lens [53].

#### 2.1.2. Targets

On the movable parts of the windows and shadings, rectangular targets are installed to provide a color-coded reference point for image post-processing. The target size of 30 mm × 70 mm is chosen for two main reasons: on the one hand, the area ensures good visibility. On the other hand, the target size is chosen to guarantee that the pixel resolution is sufficient to accurately detect the target apparent ratio and size when moving with the window, thus increasing accuracy. This is of particular interest for applications where the target may be deformed by rotation, e.g. when a window is tilted. Physical accuracy limits are imposed by the geometric properties of windows and shadings, the position of the camera in the room, and the resolution of the sensor. The target size is chosen accordingly to maximize precision, keeping in mind the prototype case study presented in Section 2.4. All mounted targets and monitored building services are illustrated in Fig. 2.

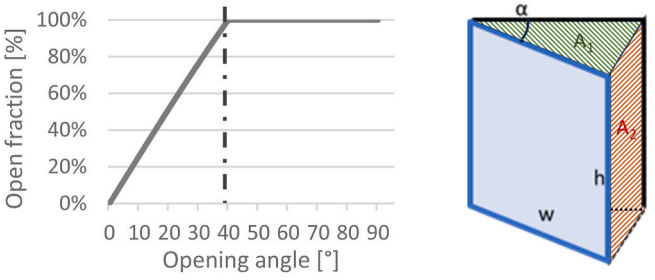


**Fig. 1.** Opening angle vs. opening fraction (of maximum air exchange area) with opening angle α, opening distance d, window open area A, for a European-style left-hinged window according to Ref. [30].

### 2.2. Post-processing algorithm

The target recognition algorithm is coded in Matlab (Matlab R2022b, 2022) using tools from the image post-processing toolbox. The post-processing algorithm is used to extract the information contained in the images obtained by the experimental setup. Once the camera is mounted, images are taken at predefined window positions to calibrate the device and account for the characteristics of the monitored room. These calibration images are taken for each window in fully closed (0°), partially open (30° and 60°), and open (90°) configurations. They are used to determine the coordinates of the targets on the sensor's pixel pane when closed and fully open, which is needed to calculate the parameter $d_{90}$ used in Equation (1). In addition, a Region of Interest (ROI) is defined for every building service to ensure full visibility of the target trajectory. To maintain the occupant's privacy, images are immediately post-processed, and only the data are stored and made available for export or download. Only for verification purposes, full images are kept in the initial phase and a privacy shield is deployed in front of the camera instead. It comprises a wooden physical barrier that obstructs the camera's direct line of sight to the occupied section of the classroom. This arrangement restricts the camera's view to only the movable components, such as windows, shades, and lights, ensuring privacy protection in the occupied area.

#### 2.2.1. Target recognition

As described in Section 2.1.2, color-coded targets are chosen as reference on the moving parts of the monitored objects or the luminance – indicated by the V value – for the state of the artificial lighting. The color codes used are red for windows and green for shades. To find only the colored areas of an image, the post-processing algorithm is set to filter all pixels for specific values. In the current development stage, the problem of color identification under different illumination conditions could be overcome by transforming the RGB pixel color values into a more suitable color space for recognition purposes. The HSV color space is well illustrated by Cheng et al. [54]. The HSV color model has been developed in analogy to the human visual perception (Valín & Alberto J. V., 2019) dividing an image into color perception (Hue), color intensity (Saturation) and light intensity (Value). Every color is represented in all variations within a certain hue range including darker, lighter and slight variations of the color tone. The HSV color space can be thought of as a mirrored cone like shown in Table 1 where the height of the cone represents the illumination value with black at the bottom tip and white at the top. From the cone a disk can be cut where each point is defined by an angle (Hue) and the distance from center (Saturation).

The fundamental advantage of the HSV color space compared to the RGB color space is that it makes it very intuitive to specify the color within a very narrow range of hue independent of the illumination conditions. In a test series shown in Section 3, the standard deviation of hue values for red in varying illumination resulted to be negligibly small compared to the RGB values. The pixels identified as being within the specified hue range are stored in a matrix of the same dimensions as the image, referred to as *mask*. The hue categories are taken from a Python Plug-in OpenCV 4 which is further explained in Valín & Alberto J. V. (2019) [55]. The used categories are shown in Table 1.

In a next step, noise (i.e., an area smaller than 200 pixels) is removed from the mask. To verify that the mask matches the target on the window, the geometry, size, and color ratio of the mask is checked. The aspect ratio of the selected targets is 0.43. Due to distortion depending on the cameras point of view an aspect ratio range between 0.39 and 0.47 is accepted as valid.

Lights result in a V value over the threshold of 0.9 when turned on,


**Fig. 2.** Camera perspective on the room used for prototyping including targets (left), assembled device (right).

**Table 1**
HSV color range used for post processing (left) & graphical representation of HSV color space (right) (adapted from Valín & Alberto J. V., 2019).

| Color | Hue [°] | Saturation [-] | Value [-] |
|---|---|---|---|
| Red | 0 – 10<br>160 -180 | 100 - 255 | 20 - 255 |
| Green | 55 - 75 | 100 - 255 | 20 - 220 |
| Overexposed (Lights) | 0 -180 | 0 - 255 | 190 - 255 |

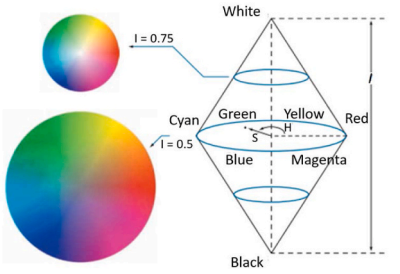


indicating overexposure. Overexposure occurs when too much light reaches the camera's sensor. It means that the image is too bright and appears white in the affected area. Overexposure due to artificial light is notably stronger with V values exceeding 0.9, a threshold that natural sunlight cannot attain within the Region of Interest (ROI) for the here presented case study. The yellow targets seen in Fig. 2 have been used to study color recognition with respect to the yellow background environment elements but have not been used in this post-processing algorithm.

### 2.2.2. *Calculation of window angle & shading position*

If the mask passes the verification of the aspect ratio and area, it is successfully recognized as a "target" within the monitored area. Otherwise, the post-processing algorithm prompts for manual user input, which was reduced to around 1% (using HSV color space) with respect to previously 5% using RGB values and illumination categories [39], depending on the post-processed building service. After the target is detected, the algorithm reads the coordinates of the target center and compares them with the coordinates of the window or shading in the closed state. Then, the distance in pixel between the identified target position and the target in the closed state is used as identification value d. To convert this pixel value, the following equations are used for the window angle (1) and the shading position in terms of height (2) or percentage of aperture (3):

$$\alpha = acos(1 - d / d_{90}) \tag{1}$$

where $d = x_{measured} - x_{closed}$ with $d_{90}$: distance in pixels if window fully opened, $x_{measured}$: current coordinates of target, $x_{closed}$: coordinates of target if closed

$$S_x = (x_{measured} - x_{closed}) * H \tag{2}$$

$$S_{\%} = S_x / H \tag{3}$$

where $x_{measured}$: current coordinates of target, $x_{closed}$: coordinates of target if shading closed, *H:* height of window.

For multiple-sash windows, as in the considered case, each sash is provided with a target and its position is analyzed individually.

The retrieved information on angle, position or status is associated with the date and time in the image's metadata and finally written to a CSV file for further evaluation. The *main* code calls subfunctions to analyze windows, shadings, and lights separately in detail.

The post-processing steps listed above are illustrated in the flowchart in Fig. 3 for the window state detection algorithm. The processing starts with the *main* code and proceeds step by step, calling subfunctions as *SenseWindow* that perform the actual target recognition as shown.

## 2.3. *Accuracy constraints*

Several parameters of the developed device affect the achievable accuracy. The main accuracy constraints are imposed by the sensor resolution, the target recognition algorithm, the geometrical properties of the monitored room, and the lens distortion.

To test the device's accuracy, a controlled test series is analyzed where windows are progressively opened at 18 predefined angle values (Dataset A), all directly measured on-site with a tape measure. The

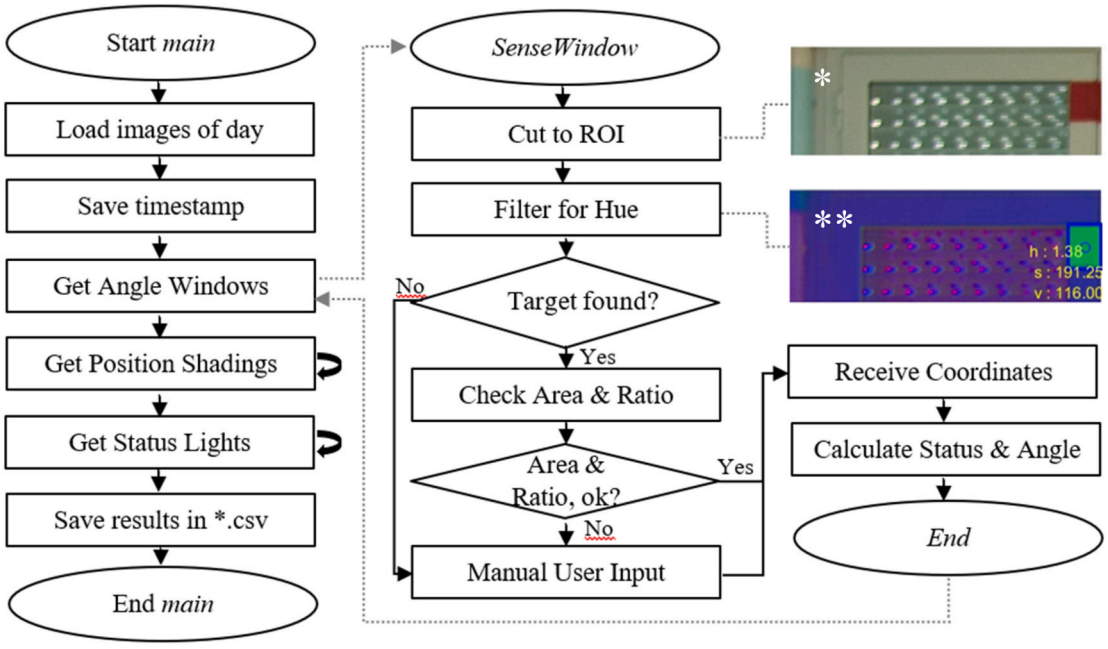


**Fig. 3.** Flow chart showing the HSV image post-processing algorithm, the ROI for window 1 (*) and its conversion to the HSV color space (**). (For interpretation of the references to color in this figure legend, the reader is referred to the Web version of this article.)

device is then used to monitor the angle. The results obtained during the controlled test series are analyzed with and without (i) geometrical and (ii) distortion corrections to assess their respective impact. Knowing the exact opening angle in the controlled test series allows immediate traceability of accuracy in terms of relative and absolute measurement errors. The images of the controlled test series are obtained for the same reference room as used for the proof of concept outlined in the following Section 2.4. The test images are furthermore used to calibrate a digital grid that can be overlaid on any images taken in the same room to obtain accurate opening angles. The digital grid is thus used to verify the results obtained during the proof of concept.

### 2.3.1. Sensor resolution and target recognition algorithm

The physical accuracy limits imposed by the sensor resolution are given by the horizontal distance traveled by the target depending on the opening angle/position and corresponding pixel resolution as further discussed in Section 3.1.1. The distance traveled by the target measured in pixels is determined apart from the sensor's resolution by the ability of the target recognition algorithm to capture repeatedly the center of the target under varying conditions and opening angles. The sensitivity of these constraints on the angle measurement can be represented as a specific correlation depending on the room size, target size, and sensor resolution. Results for the here presented sensor and case study are shown in Section 3.1.

### 2.3.2. Geometrical properties of the monitored room

Additional inaccuracies are mostly due to geometrical reasons, especially the position of the camera with respect to the swiveling trajectory. An idealized setup would be mounted straight in front of the target to be monitored, as shown in image (c) of Fig. 4. Since most applications involve the observation of multiple targets in a physically limited space, the camera is often placed at a certain offset angle Θ′, as described below. This angle Θ′ characterizes the geometric correction for each window according to Equations (6)–(8).

Geometric properties of camera-to-window position:

$$\Theta' = tan^{-1}\left(\frac{\Delta\,WW}{\Delta\,CW}\right) \tag{4}$$

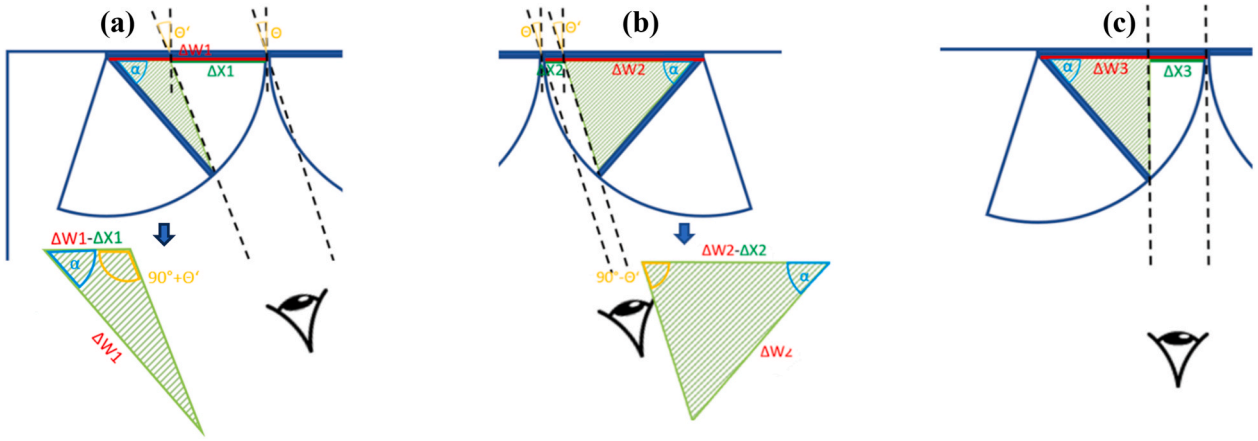


**Fig. 4.** Geometric properties of the camera to window (or sash) position, indicated by Θ'. (a) Left hinged window monitored from the side, (b) right hinged window monitored from the side, (c) window positioned in front of camera.

Straight view on the window:

$$\alpha = \cos\left(\frac{\Delta W3 - \Delta X3}{\Delta W3}\right) \quad (5)$$

Left hinged window seen from the side:

$$\alpha = 90^\circ - arcsin\left(\frac{cos(\Theta')}{\Delta W1} * (\Delta W1 - \Delta X1)\right) - \Theta' \quad (6)$$

Right hinged window seen from the side:

$$\alpha = 90^\circ - arcsin\left(\frac{cos(\Theta')}{\Delta W2} * (\Delta W2 - \Delta X2)\right) + \Theta' \quad (7)$$

Limitations due to swiveling trajectory:

$$\alpha_{lim} = 180^\circ - 2*(90^\circ - \Theta') = \Theta' \quad (8)$$

The reference room and the parameters referred to in this paragraph are shown schematically in Fig. 5. The offset of each window is described by the parameter Θ′ according to Equation (4), where ΔCW is the shortest distance from the camera to the opposite wall and ΔWW is the distance from the center of the wall to the hinge of the monitored window. For windows positioned in front of the camera, the measured pixel displacement of the target can be converted to an angle using Equation (5). However, for the remaining windows, the camera's view is typically from the side, which results in the need for a correction factor that accounts for the geometric correction of the angle considering the window's hinge (center of rotation) as reference point defined by Θ'. For left-hinged windows, Equation (6) can be used, and for right-hinged windows, Equation 7is appropriate.

Windows facing the camera with their hinges show a limiting angle $\alpha_{lim}$ due to the swiveling trajectory, which cuts the theoretical line of sight from the target to the camera. Basically, in this case, the camera sees the target becoming slightly larger, but not moving horizontally to the right or left. The critical angle is reached when the target moves in front of the indicated "closed position" and the open window is indistinguishable from a closed window. This is shown schematically in Fig. 4 (b). The calculation of $\alpha_{lim}$ shows that it is equal to the geometrical property parameter Θ′ as shown in Equation (8).

### 2.3.3. Lens distortion

Typically, various mathematical models can be used to correct for lens distortion [56]. Often, they are pre-built into software packages that are capable of correcting images for all lens-induced effects. For the present case, however, since only one-dimensional distortion is of interest, simpler equations are used and calibrated with a dedicated sample image. Either a 4th-order polynomial or a simplified 3rd-order polynomial can be considered for distortion correction. The lens-specific factors a, b, c, or $k_1$ are found empirically using a calibration image with a grid that is adjusted until equal grid spacing is achieved. For the given application equation (10) is used.

4th order polynomial:

$$R_d = a * R_u^4 + b * R_u^3 + c * R_u^2 + (1 - a - b - c) * R_u \quad (9)$$

Simplified 3rd order polynomial:

$$R_d = k_1 * R_u^3 + (1 - k_1) * R_u \quad (10)$$

where $R_u$ is the distance of the undistorted pixel and $R_d$ is the distance of the distorted pixel. For the specific lens used for the proposed device, the correction factor *k1* is found to be 1.5 $10^{-6}$.

### 2.4. Proof of concept & long-term field study

To ensure the functionality of the device, a preliminary comparison is made between the manually measured ground-truth data and the results obtained by the proposed post-processing algorithm using 50 test images. The detailed dataset used for accuracy assessment, validation, and proof of concept and its evaluation has been presented in Donges et al. [39]. The dataset examined in this context is part of a large-scale monitoring campaign aiming to fully understand the different aspects of IEQ in schools, the interactions of teachers and students with building services, and the impact of safety measures adopted to prevent viral infection on performance, comfort, and behavior. The measurement campaign included long-term monitoring of six naturally ventilated classrooms in a secondary school in Morlupo, Italy, from December 2021 to June 2022. It needs to be noted that this time has been during the COVID pandemic which draw special attention to ventilation and might have effects on the presented behavior. The device presented here was installed for testing purposes in one of the classrooms whose layout is shown in Fig. 5. The floor area is about 50 $m^2$ and each classroom is equipped with three two-sash windows, each with airtight roller-shutters that close from top to bottom (Cd = 1), and ceiling mounted fluorescent lamps. The sashes are named from left to right and are abbreviated as *Win1* to *Win6*. To avoid confusion between sash and shade, the window sashes are named *Win1&2* representing the two sashes of the left window, *Win3&4* for the middle, and *Win5&6* for the two sashes of the right window. The shades are similarly named from left to right as *Shade 1* to *Shade 3*. As for lighting, each room is equipped with

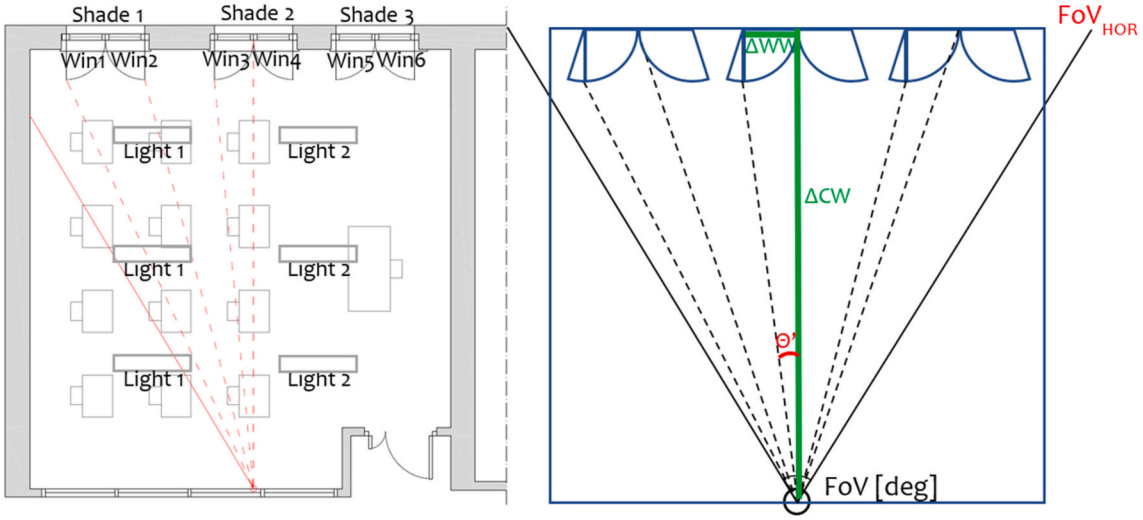


**Fig. 5.** Floorplan of classroom chosen for case study and nomenclature windows & parameters.

four light bodies controlled by two switches. The lights on the left (near the back wall) are labeled *Light 1*, and those on the right (near the teacher's desk) are labeled *Light 2*. The naming and relevant room geometries are shown in Fig. 5.

During the field-study images have been acquired in a timestep of 10 min of all mentioned building services and targets which should be acknowledge when using the data to develop behavioral models. The chosen 10-min timestep has been deliberately selected to ensure enough time for reliable processing even with microprocessors. Only working hours from 8 a.m. to 3 p.m. have been monitored. Functionality could be observed remotely as well as through the download of the obtained data. The dataset has been elaborated to calculate the resulting air exchange area as shown in Section 1 which is relevant for ventilation properties. For windows and shades, the predicted status, angle and position is measured. The status measurement is defined as the binary state open/close or on/off. As angle or position the continuous measurement of window angle and shade position is meant. Environmental data like indoor temperature, relative humidity, $CO_2$ concentration, and outdoor temperature are added to the dataset. From this data the hourly, daily and weekly averages have been calculated. Further the continuous air exchange area is obtained using the windows angle and shading position. Also, the binary air exchange area is added to showcase the merits of continuous monitoring by confronting them with a binary alternative. The status closed has been assigned in the measurement range of 0°–3° opening of windows. Here it has been assumed that for windows opened $> 3°$ the contact sensor is not closed (and therefore opened at 90° in a binary world). Shades are assumed to close the contact sensor when fully lowered, meaning every shade not fully lowered is considered as completely opened.

## 3. Results

After the design process of the proposed monitoring tool, including its post-processing approach, a preliminary test series and a long-term study were conducted to gain insight into the optimal configuration of hardware components, targets, the post-processing algorithm and range of application and merits of the proposed solution.

The hardware components aim to provide the highest image quality and field of view to capture the maximum number of details, which is important for the development stage of the post-processing algorithm. Regarding the targets, color recognition is more reliable than identifying the geometric shape of objects because color-coded targets are more unique. In addition, overexposure can be used for the monitoring of lights, which is not possible by the recognition of geometric properties but by reading the HSV values of pixels. Hence a consistent post-processing approach is chosen. It is to mention that the choice of a unique color - not being present in the environment contained in the image - is essential. The choice of the post-processing approach is related to the previous choice of suitable targets for the given application.

After the basic hardware and software components have been evaluated in Section 2.1, accuracy and reliability are assessed in two steps: (i) by determining the measures that affect accuracy in a controlled test environment, and (ii) by validating the device using the data from a 6-month prototyping case study mentioned in Section 2.3.

### 3.1. Determination of accuracy in controlled test environment

For accuracy assessment, dataset A is used. In dataset A, windows are opened in 18 discrete steps at predefined angles from 0° to 90° and the opening angle is measured physically on site. The resulting image series is post-processed with and without the application of the geometry and distortion correction formulas and compared to the physically measured value as described in Section 2.4. The test series is performed for each window separately, while a clear symmetry between *Win1* & *Win6*, *Win2* & *Win5*, and *Win3* & *Win4* is observed, given the geometry of the room. Therefore, only *Win1*, *Win2* and *Win3* - as defined in Fig. 5 - are presented in the following.

Using this controlled test environment, four intrinsic factors are examined that govern the accuracy of the device: (i) the resolution of the camera sensor, where adjacent pixels allow to identify only discrete target motion steps, (ii) the target recognition algorithm, (iii) geometrical factors imposed by the camera position, window swivel trajectory, and general spatial conditions in the room, and (iv) lens distortion. Assuming that the impact of sensor resolution, target detection, geometric correction, and lens distortion (i - iv) do not affect each other, the influence of each can be quantified as shown in Fig. 7. Adding the exact opening angle to the measurement results allows us to immediately evaluate the accuracy in terms of relative and absolute measurement errors. The sum results in the overall accuracy achieved in the controlled test environment, as presented in Table 2. Given that the measurement error is mostly systematically present over all test images, it can be corrected by geometrical and distortion correction factors which are empirically found. Just the errors caused by the sensor resolution are of stochastic nature but are negligibly small ($< 0.5°$) for angles greater than 20°. Given that angles greater than 20° represent over 80% of dataset A, a systematic correction using the presented correction factors, leads to promising results. These results and correction approach is discussed in the following and shown in Fig. 7.

#### 3.1.1. Inaccuracies imposed by the camera sensor resolution

Assuming a horizontal field of view of about 5.09 m as given in the case study, each pixel of the 4056 pixel wide sensor represents a horizontal target movement of 1.3 mm. Therefore, each pixel resolves into 1.3 mm of real distance traveled, which translates into a varying angular offset Δα as shown in Fig. 6, assuming a window positioned in front of the camera as shown in Fig. 4(c). Opening angles greater than 15° show a negligible offset of less than 0.5°, while smaller angles can only achieve accuracies between 4° for very small opening angles and no better than 0.5°. The imposed inaccuracies due to target recognition and geometric properties of the camera and window/shade positions are tending to be more significant.

#### 3.1.2. Inaccuracies imposed by the target recognition algorithm

At the pixel level, other inaccuracies can be associated with the target recognition algorithm. The boundaries of the colored target and the corresponding target center coordinates vary by a few pixels depending on the opening angle during target acquisition. This is due to variations in lighting conditions and geometric deformation of the target if rotated or partially covered, resulting in a random offset that fluctuates around the actual target center. If the target center is offset by a certain number of pixels, a theoretical calculation can quantify the offset as an angle accuracy limit per pixel, as shown in Fig. 6, assuming a window positioned in front of the camera shown in Fig. 4(c). This implies that the accuracy is very limited, especially for smaller angles. The influence of target recognition is quantified by subtracting the inaccuracies caused by geometrical properties and lens distortion as shown in Sections 3.1.3 and 3.1.4.

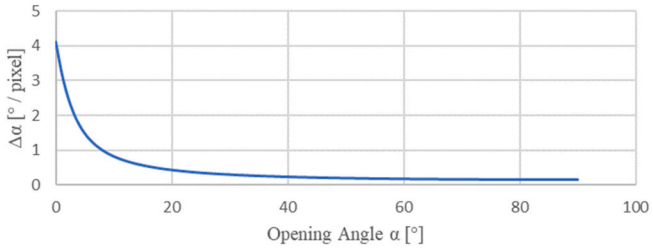


**Fig. 6.** Theoretical accuracy limited by sensor resolution in degree per pixel depending on the opening angle.

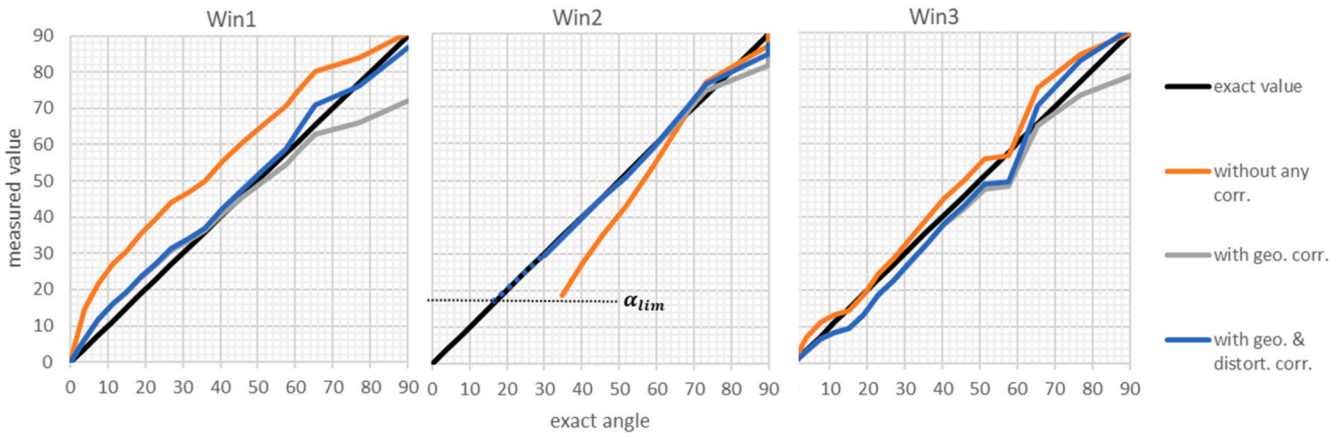


**Fig. 7.** Comparison of the measured angle without any correction (orange), with geometrical correction (grey), and with geometrical & distortion correction (blue), to the exact value (black). (For interpretation of the references to color in this figure legend, the reader is referred to the Web version of this article.)

**Table 2**
Mean absolute and relative accuracy with respect to angle range and correction formula applied.

| Win1 | without any Corr. | | with geo. Corr. | | with geo. & distort. Corr. | |
|---|---|---|---|---|---|---|
| Angle | Mean Abs. Err. | Mean Rel. Err. | Mean Abs. Err. | Mean Rel. Err. | Mean Abs. Err. | Mean Rel. Err. |
| 0° < α < 90° | 11.75° | 55% | 5.93° | 17% | 2.79° | 14% |
| α < 45° | 15.31° | 104% | 3.09° | 25% | 3.50° | 26% |
| α > 45° | 8.90° | 15% | 8.20° | 10% | 2.21° | 3% |
| **Win2** | | | | | | |
| Angle | Mean Abs. Err. | Mean Rel. Err. | Mean Abs. Err. | Mean Rel. Err. | Mean Abs. Err. | Mean Rel. Err. |
| 0° < α < 90° | 4.08° | 13% | 1.93° | 3% | 1.53° | 3% |
| α < 45° | 5.03° | 57% | 0.16° | 1% | 0.15° | 1% |
| α > 45° | 3.32° | 5% | 3.35° | 4% | 2.63° | 3% |
| **Win3** | | | | | | |
| Angle | Mean Abs. Err. | Mean Rel. Err. | Mean Abs. Err. | Mean Rel. Err. | Mean Abs. Err. | Mean Rel. Err. |
| 0° < α < 90° | 3.29° | 12% | 5.00° | 13% | 3.63° | 11% |
| α < 45° | 2.48° | 20% | 3.46° | 18% | 3.36° | 17% |
| α > 45° | 3.94° | 6% | 6.23° | 9% | 3.84° | 6% |

#### 3.1.3. Inaccuracies imposed by geometrical factors

Geometrical factors imposed by camera position, swiveling trajectory, and room geometry can be balanced by applying $\Theta'$ as a correction factor, according to Equations. (6) and (7). The limiting angle $\alpha_{lim}$, as described in Section 2.3.2, has been calculated to be 18.4° for *Win2*, while *Win1* and *Win3* show no limitation due to the geometrical properties or the swiveling trajectory. The effect of the geometric properties of the window-to-camera position is visualized in Fig. 7 as a comparison of measurements that are corrected using Equations. (6) and (7) (grey), applying $\Theta'$ as the correction factor as shown in Section 2.3.2, and measurements that are not geometrically corrected (orange). The more the angle of observation deviates from normal incidence, the more significant is the geometric correction. *Win1* shows the greatest response to the geometric correction, while *Win3* shows the least, since it is positioned in front of the camera. This trend is visible in Fig. 7, looking from left (*Win1*) to right (*Win3*).

#### 3.1.4. Inaccuracies from lens distortion

The angle measurements obtained in the controlled test environment show that lens distortion is increasingly important for angles greater than 45°. Since the number of pixels traveled per degree of opening increases significantly in this angle range, an accurate pixel width is more important than for small angles. To account for the distortion, the third-order polynomial equation shown in Equation (10) is applied with a correction factor *k1* of 1.5 $10^{-6}$ as explained in Section 2.3.3. Applying Equation (10) to the provided data can remove the effects of lens distortion. For angles greater than 45°, the distortion correction can reduce the relative error in angle measurement from 10% to only 3%, as shown in Table 2. The remaining 3% is related to inaccuracies in the target recognition algorithm.

The average of the relative and absolute measurement errors leads to the overall accuracy achieved in the controlled test environment as shown in Table 2. For example, in the case of *Win1*, an overall mean absolute error for window opening angles of 2.79° (14% mean relative error) is achieved. The main source of inaccuracy are small opening angles. If we consider only angles larger than 45°, the accuracy of the device improves significantly to a mean absolute error of 2.21°, which corresponds to a mean relative error of only 3%. This trend is confirmed for *Win3*, whereas *Win2* shows a better accuracy for angles < 45°, due to the negligence of angles smaller than the limiting angle $\alpha_{lim}$. Therefore, the geometric and distortion correction is able to reduce the mean error to an acceptable minimum of about 2°–3°.

### 3.2. Long-term case study

To validate the concept and design of the presented monitoring device, the here presented work focusses on the analysis of the full 6-month data set which, in conjunction with other sensors measuring environmental data, provides a complete picture of the behavioural and ventilation patterns in the monitored classroom. The resulting general dataset consists of information on windows angle, shading position, light status, door status and ambient data such as indoor temperature, relative humidity and $CO_2$ concentration as well as outdoor temperature and humidity obtained in discrete timesteps of 10 min. The follow-up analysis presented here consists of the demonstration of the hourly and weekly evolution of the air exchange area in time. Furthermore, every building service has been analyzed regarding patterns in the usage. Special attention has been paid to the windows as primarily analyzed building service. The results obtained using the proposed post-processing algorithm are confronted with the results obtained if a binary sensor would have been used.

#### 3.2.1. Windows

It should be noted that 88% of false measurements occurred at opening angles less than 20°. These inaccuracies at small aperture angles are due to the reasons described in Section 3.1, i.e. small aperture angles lead to higher sensitivity due to reduced target movement per aperture angle. In addition to the geometrical constraints imposed by the limiting

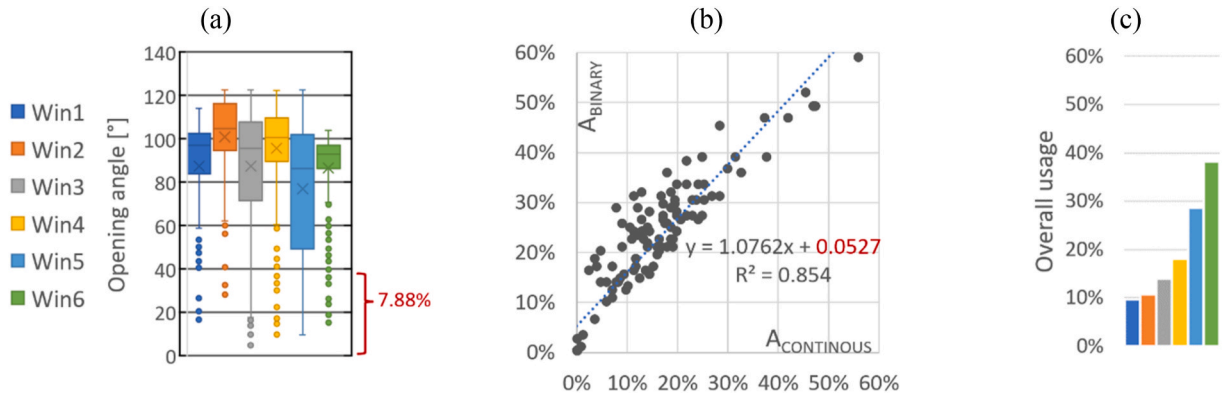


**Fig. 8.** Analysis of windows for 6-month monitoring campaign. (a) Boxplot of opening angle if in use, (b) Daily average exchange area (in % of $A_{max}$) as binary (y-axis) and continuous result (x-axis), (c) Overall window use during working hours.

angle $\alpha_{lim}$, slightly opened windows (< 20°) are generally considered critical events for monitoring with the proposed device. There is also evidence that large angle measurement errors are caused solely by windows 2 and 5. Here, the main cause of the increased number of errors on windows 2 and 5 are the geometric constraints imposed by the camera position and the window swiveling trajectory reduced by the limiting angle $\alpha_{lim}$. These deviations only consider the post-processing error and not the errors defined in Sections 2.3.1 - 2.3.3.

The long-term analysis revealed insights in the operation of the individual window sashes. Note that all window sashes, shades, and lights are labeled as in Fig. 5 and their state is measured in discrete timesteps of 10min. The general observations for the particular case of the High School of Morlupo are shown in Fig. 8. The mean opening angles are quite high: on average 88° for window 1, 101° for window 2, 88° for window 3, 96° for window 4, 77° for window 5, and 87° for window 6. Furthermore, 75% of all opening events show larger opening angles between 80° and 120°. Whereas only 7.88 % of all opening events are in the relevant angle range between 0° and 40°. These small angles impact the air exchange area which already reaches its maximum at an aperture angle of 40° as shown in Fig. 1. Furthermore, as can be seen in Fig. 8, windows closer to the teacher's desk are operated more frequently and in general the window sash on the right side of each individual window is operated more frequently due to the opening handle mounted there.

Comparing the binary with the continuous exchange area (averaged for the entire room based on the position of all sashes and accounting for the shades position) shows a constant offset of around 5 % overestimate if binary sensors would have been used which is in the same magnitude of the percentage of opening events in the relevant angle range (0°–40°), with a proportional inaccuracy factor of 7.6 % of the continuous value. Despite aligned blind angles (geometric constraints as explained in section 3.2.1) leading to matching opening areas between continuous and binary measurements, the considerations outlined contribute to an overall 5% improvement in the accuracy of the opening area estimation.

### 3.2.2. *Shades*

A previously performed proof of concept revealed that the shades show the lowest rate of wrong measurements of all building services due to the simple geometric concept of a purely vertical moving target as opposed to a rotating target such as those fixed on the windows. During the here presented six-month monitoring period, shade 1 is on average lowered 43%, shade 2 at 38% and shade 3 at 54%. The mean shading position during working hours ranges mostly in between 20% and 80% and is shown as weekly average in Fig. 11 (middle). The fact that shades rarely fully close, highlights the more precise representation using the continuous image-based approach, especially in scenarios with partial closure. For the shades the same tendency as for the windows can be seen with the shades closest to the teacher's desk being used the most.

### 3.2.3. *Lights*

Light 1 & 2 represent the two light bars at the back and front of the room as seen in Fig. 5. They are controlled separately by two switches. The long-term analysis of the lights revealed that the average usage time declines towards the summer month given the greater availability of natural light. This trend is shown in Fig. 9 which shows the weekly average time of light usage.

## 4. Discussion & merits of proposed device

After accuracy assessment and validation, the merits of the proposed device can be discussed by processing larger amounts of data acquired during the pilot study. During acquisition, the time step is set to 10 min to match the time step typically used in building simulations. The monitored data can be visualized on a daily basis as a continuous timeline containing all acquired data as exemplary shown in Fig. 10. In these daily data visualizations, it is evident that each window opening event (continuous lines in Fig. 10) results in an air exchange area (light & dark grey area in Fig. 10) which is calculated using the opening angle and the shading position (dashed lines in Fig. 10). The data related to the

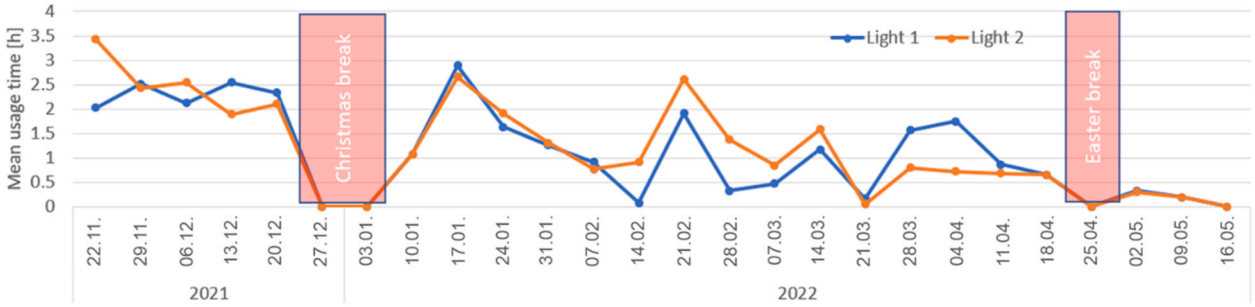


**Fig. 9.** Weekly mean time lights are turned on during working hours.

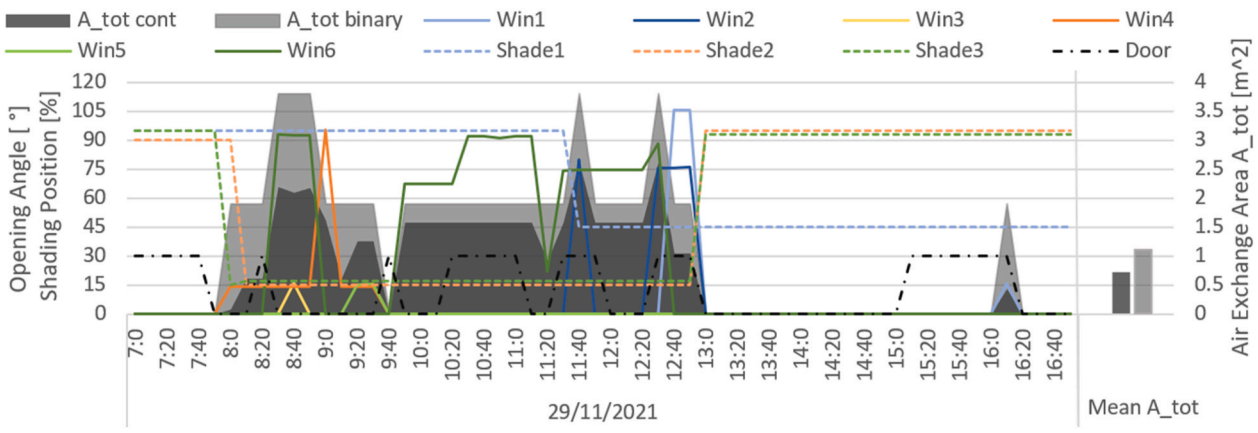


**Fig. 10.** Binary (light grey area) vs. continuous (dark grey area) air exchange area (A_tot) - 29/11/2021.

door opening is retrieved by the contact sensor plugged into the device as described in Section 2.1.1. All window and shading measurements are combined to calculate the corresponding air exchange area $A_{tot}$ between the in- and outdoor environment in a binary way (windows opened 0° or 90°; shading lowered 0% or 100%) or continuous way using the obtained data delivered by the device.

Since the ventilation rate is proportional to the free opening area according to the norm EN 16798-7:2018 [29], we can draw conclusions about the ventilation rate and compare it with the results obtained if, for example, contact sensors had been used to obtain binary information about the use of windows and blinds. From Fig. 10 it is evident that the binary exchange area (light grey) typically overestimates the continuous exchange area (dark grey). Each day can be summarized to a mean air exchange area $A_{tot}$ presented on the right side of Fig. 10. Similarly, weekly mean air exchange areas are calculated and shown on the bottom in Fig. 11. The confrontation of continuous to binary results illustrates that detailed measurement of building services can have a fundamental impact on ventilation strategies, assumed IEQ, and retrofit strategies.

To test the newly developed device extensively, it has been used in a school for 6 months as described in section 2.4. The data is analyzed to draw qualitative and quantitative conclusions. Fig. 11 shows the weekly averages of the window aperture angles, shading positions and confronts continuously measured with binary measured air exchange area over the entire 6 months. The windows and shades show no seasonal trends but clearly are not used during holiday times. Also, the overall air exchange area – which has been expected to increase with warmer temperatures – has been quite constant throughout springtime with a rapid increase towards the beginning of summer from 16.05.22 onwards. The stated result could have been influenced by the presence of COVID measures to ensure ventilation in classrooms, e.g., special attention of the teacher to proper ventilation (most frequent use of window 6) or steady ventilation requirements (no seasonal trends).

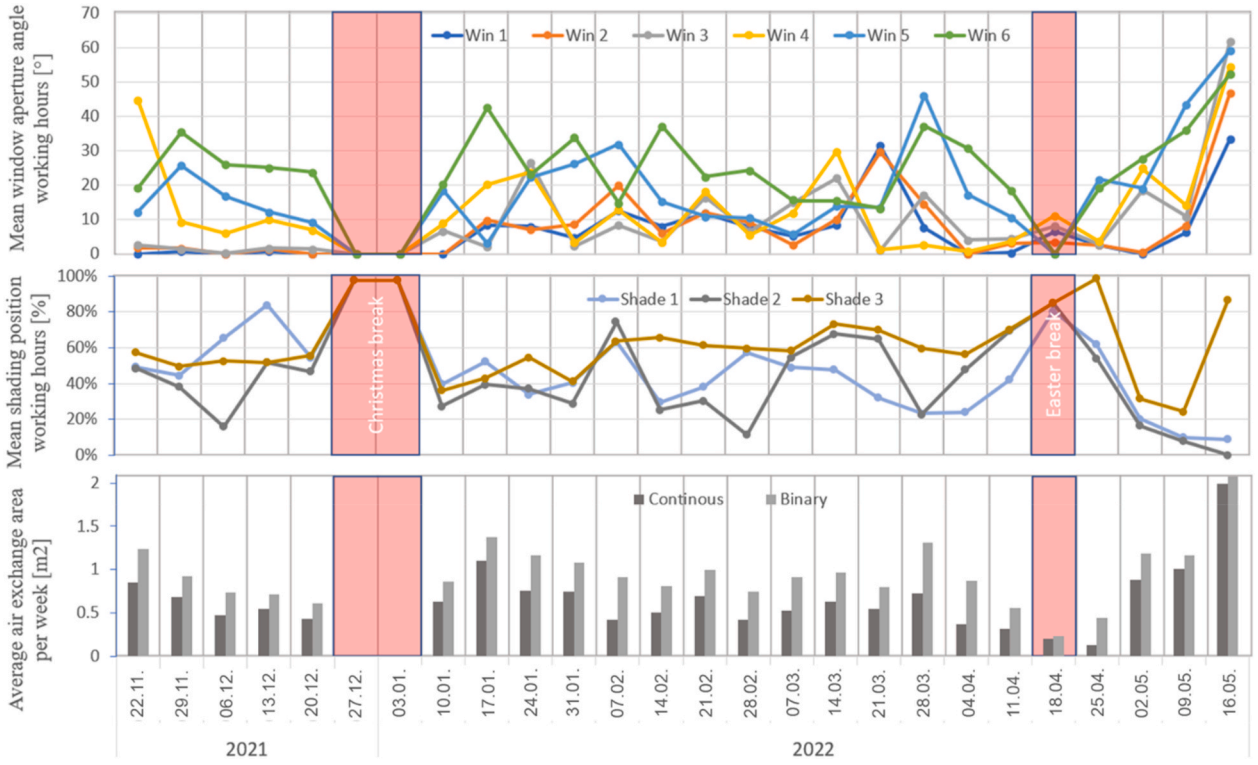


**Fig. 11.** Quantitative representation of long-term monitoring. Weekly averages are shown of aperture angle (top), shading position (middle) and continuously measured vs. binary measured air exchange area (bottom).

It is one research goal to outline the strength of the device - the continuous observation – which makes it possible to determine the exact air exchange area and to compare it directly with its binary measured counterpart. The trend stated in Section 3.2.1 can be confirmed as the binary results overestimate the ventilation rate constantly. The overall mean opening area considering all datapoints shown in Fig. 11 is 0.60 $m^2$ when measuring continuously and 0.87 $m^2$ when measuring in binary mode. This represents an actual overestimate of 45% of the air exchange area. This error can be higher for slightly opened windows which usually occur in winter times with colder outdoor temperatures favoring air exchange (stack effect) and higher wind speeds (wind effect). These three driving factors support the accurate and continuous measurement of window opening angles and shading positions. Especially, in times of COVID where sufficient ventilation is crucial for well-being, overestimated ventilation properties can be misleading. Thinking one step further, the development of accurate behavioral models can profit from the usage of this device, delivering accurate continuous data on behavioral patterns.

## 5. Conclusion

The present study reports the development of a camera-based device capable of monitoring multiple windows, shadings, and lights simultaneously. Its main feature is the ability to measure opening angles and shading positions for a detailed estimation or modeling of the natural ventilation rate in a room or to support the development of occupant behavior models, while This dataset was acquired during a 6-month monitoring campaign in a school building, specifically in a classroom. The single-room approach, while providing targeted data, stands out for its simplicity, cost-effectiveness, and privacy advantages, making it valuable for both research and practical applications. The ability to obtain detailed information on window angles and shading positions is a beneficial alternative to conventional methods with binary output (open vs. closed). To the authors' knowledge, these methods for detailed monitoring of angles and positions have not been fully explored in the literature yet.

In this research proceeding, a suitable post-processing, and deployment of the device in a case study has been realised, to showcase accuracy, reliability, functionality, and the merits of the proposed device. For image post-processing, a color recognition algorithm has been chosen that detects color-coded targets using the HSV color space. The main feature is the ability to identify predefined colored targets mounted on the moving parts of windows and shades, and its suitability for monitoring lights. Great attention has been paid to privacy issues, which is ensured by a strict image reduction to the necessary ROI and elimination of the image after automatic post-processing.

The accuracy of the device and the algorithms is evaluated using a controlled test series of 18 images (Dataset A) with ground truth angle and shading position measurements. In particular, the impact of sensor resolution, target detection, geometrical correction and lens distortion has been evaluated (i - iv, Section 3.1). The controlled test series therefore results in an accuracy evaluation, which is presented as mean relative measurement error in %. In the case of window measurements, the average relative measurement error over all measured window angles is 27 % without any correction. This could be significantly improved to 11% by applying geometrical correction factors and even to 9% by further applying distortion correction. It is worth noting that angles smaller than 45° are more prone to measurement errors with a relative error of 14.6% compared to larger opening angles with only 3%.

Moreover, possible analysis scenarios of the data obtained during the long-term monitoring are presented, highlighting behavioral trends such as the most frequent use of the window sash closest to the teacher's desk or the less use of the lights towards summer. If we confront the potential binary results to the obtained continuous ones, it is evident that binary sensors clearly overestimate ventilation. In the present monitoring campaign, windows could not be opened in tilt mode (0–20° vertically) but just in turn mode (0–120° horizontally). Additionally, the mean opening angles using all datapoints for each window are quite high ranging around 80°. However, the opening events below 40° which occurred in 7.88 % of all cases, had a strong effect on the air exchange area and accordingly on the ventilation rate. Continuous measurements are benchmarked with their corresponding binary measurements which resulted in an overall offset of more than 5.27 % which is in the aforementioned magnitude of the percentage of opening events in the range below 40°. It is assumed, that the angle measurement is more important for windows which can be operated in tilt & turn mode given the higher frequency of low opening angles.

The analysis revealed some limitations of the window angle measurement approach that need to be further addressed. Limitations in image resolution can be easily overcome by an appropriate choice of sensor and lens setup according to the room dimensions combined with an adapted lens distortion correction. On the other hand, limitations related to the geometric properties of the room, especially the trajectory of the window opening with respect to the camera position in the room, are not easily resolved. A target rotating towards the camera has a very small horizontal movement, resulting in higher inaccuracies and a minimum angle $\alpha_{lim}$ as measurement limit. In addition to these geometrical factors, due to the slower horizontal movement of the target, small opening angles show a reduced pixel resolution per angle, which leads to a decrease in accuracy if windows are only slightly opened. Therefore, opening angles $< 15°$ are considered critical measurement events and require careful handling, e.g., if a very small opening angle occurs in a single time step, but windows are closed before and after the event, the measurement is prone to be incorrect. This can be resolved integrating contact sensor as detector for small opening angles if advanced accuracy constraints are given.

The particular strong points of the device are the simultaneous non-intrusive monitoring of multiple windows, shades, and lights at once, next to the ease of installation. The previous limitations regarding the need for various illumination categories while post-processing, could be overcome by introducing the HSV color space. Therefore, it is a powerful tool and a valid alternative to monitor occupant behavior in different environments and ambient conditions. For the presented long-term study it has been proven to be a capable and reliable tool for detailed monitoring of building services such as window opening angles, shading positions, and light status.

Future work will address the post-processing possibilities of the data collected with the proposed device. The intended application of the device is the development of detailed behavioral models to improve the accuracy of energy performance simulations and ultimately improve indoor environmental quality. While this study primarily focuses on the development and validation of our monitoring system, future research will explore the multifaceted factors impacting ventilation dynamics, such as single-sided or cross-ventilation, and incorporating the door sensor data, to enhance our understanding of indoor environmental quality.

Another improvement is to move from the inside to the outside of a building, allowing an entire building facade to be captured and multiple windows and rooms to be monitored simultaneously, while providing a higher level of privacy. Taking the post-processing algorithm one step further could involve CNNs, which would allow the algorithm to measure the use of building services, possibly without mounted targets. An artificial intelligence approach requires some additional work due to the amount of training data needed to reliably run and develop the algorithm. While this has been beyond the feasibility of the presented long-term case study, a deployment of the presented device in similar or multiple identical rooms for larger monitoring campaigns would rise the possibility to create a large training dataset to train the AI algorithm. To ease the acquisition of training data, some parts of the dataset could be created virtually using photorealistic renderings, increasing automation and requiring limited or no manual intervention.

## CRediT authorship contribution statement

**Julian Donges:** Writing – review & editing, Writing – original draft, Visualization, Validation, Software, Methodology, Data curation, Conceptualization. **Federica Morandi:** Methodology, Formal analysis, Conceptualization. **Alessandro Prada:** Supervision, Formal analysis, Conceptualization. **Francesca Cappelletti:** Writing – review & editing, Supervision. **Andrea Gasparella:** Writing – review & editing, Validation, Supervision, Methodology, Conceptualization.

## Declaration of competing interest

The authors declare that they have no known competing financial interests or personal relationships that could have appeared to influence the work reported in this paper.

## Data availability

The data that has been used is confidential.

## References


[1] A. Litiu, Ventilation system types in some EU countries, REHVA J. 13 (4) (2012) 147–155.

[2] V. De Giuli, O. Da Pos, M. De Carli, Indoor environmental quality and pupil perception in Italian primary schools, Build. Environ. 56 (2012) 335–345, https://doi.org/10.1016/j.buildenv.2012.03.024.

[3] W. O'Brien, F. Tahmasebi, R.K. Andersen, E. Azar, V. Barthelmes, Z.D. Belafi, C. Berger, D. Chen, M. De Simone, Simona d'Oca, T. Hong, Q. Jin, D. Khovalyg, R. Lamberts, V. Novakovic, J.Y. Park, M. Plagmann, V.S. Rajus, M. Vellei, J. Zhou, An international review of occupant-related aspects of building energy codes and standards, Build. Environ. 179 (April) (2020), https://doi.org/10.1016/j.buildenv.2020.106906.

[4] S. D'Oca, T. Hong, J. Langevin, The human dimensions of energy use in buildings: a review, Renew. Sustain. Energy Rev. 81 (May 2017) (2018) 731–742, https://doi.org/10.1016/j.rser.2017.08.019.

[5] S. Gauthier, G. Giakoumis, L. Bourikas, G.M. Giakoumis, P. James, Understanding Window Behaviour in a Mixed-Mode Buildings and the Impact on Energy Performance, Architecture and Design, September, 2016.

[6] Z. Deme Belafi, F. Naspi, M. Arnesano, A. Reith, G.M. Revel, Investigation on window opening and closing behavior in schools through measurements and surveys: a case study in Budapest, Build. Environ. 143 (February) (2018) 523–531, https://doi.org/10.1016/j.buildenv.2018.07.022.

[7] J.S. Englund, M. Cehlin, J. Akander, B. Moshfegh, Measured and simulated energy use in a secondary school building in Sweden-a case study of validation, airing, and occupancy behaviour, Energies 13 (9) (2020), https://doi.org/10.3390/en13092325.

[8] G.Y. Yun, K. Steemers, Time-dependent occupant behaviour models of window control in summer, Build. Environ. 43 (9) (2008) 1471–1482, https://doi.org/10.1016/j.buildenv.2007.08.001.

[9] F. Naspi, M. Arnesano, L. Zampetti, F. Stazi, G.M. Revel, M. D'Orazio, Experimental study on occupants' interaction with windows and lights in Mediterranean offices during the non-heating season, Build. Environ. 127 (November 2017) (2018) 221–238, https://doi.org/10.1016/j.buildenv.2017.11.009.

[10] F. Haldi, D. Calì, R.K. Andersen, M. Wesseling, D. Müller, Modelling diversity in building occupant behaviour: a novel statistical approach, J. Build. Perfor. Simul. 10 (5–6) (2017) 527–544, https://doi.org/10.1080/19401493.2016.1269245.

[11] M. Jia, R.S. Srinivasan, R. Ries, N. Weyer, G. Bharathy, A systematic development and validation approach to a novel agent-based modeling of occupant behaviors in commercial buildings, Energy Build. 199 (2019) 352–367, https://doi.org/10.1016/j.enbuild.2019.07.009.

[12] M. Jia, R. Srinivasan, R.J. Ries, G. Bharathy, N. Weyer, Investigating the impact of actual and modeled occupant behavior information input to building performance simulation, Buildings 11 (1) (2021) 32, https://doi.org/10.3390/buildings11010032.

[13] P. Correia da Silva, V. Leal, M. Andersen, Occupants interaction with electric lighting and shading systems in real single-occupied offices: results from a monitoring campaign, Build. Environ. 64 (2013) 152–168, https://doi.org/10.1016/j.buildenv.2013.03.015.

[14] A. Kim, S. Wang, J.E. Kim, D. Reed, Indoor/outdoor environmental parameters and window-opening behavior: a structural equation modeling analysis, Buildings 9 (4) (2019), https://doi.org/10.3390/buildings9040094.

[15] N. Li, J. Li, R. Fan, H. Jia, Probability of occupant operation of windows during transition seasons in office buildings, Renew. Energy 73 (2015) 84–91, https://doi.org/10.1016/j.renene.2014.05.065.

[16] B. Jeong, J.W. Jeong, J.S. Park, Occupant behavior regarding the manual control of windows in residential buildings, Energy Build. 127 (2016) 206–216, https://doi.org/10.1016/j.enbuild.2016.05.097.

[17] D. Calì, R.K. Andersen, D. Müller, B.W. Olesen, Analysis of occupants' behavior related to the use of windows in German households, Build. Environ. 103 (2016) 54–69, https://doi.org/10.1016/j.buildenv.2016.03.024.

[18] V.M. Barthelmes, Y. Heo, V. Fabi, S.P. Corgnati, Exploration of the Bayesian Network Framework for Modelling Window Control Behaviour, 2017, https://doi.org/10.1016/j.buildenv.2017.10.011.

[19] J. Park, C.S. Choi, Modeling occupant behavior of the manual control of windows in residential buildings, Indoor Air 29 (2) (2019) 242–251, https://doi.org/10.1111/ina.12522.

[20] A. Wagner, W. O'Brien, IEA EBC Annex 79 Proposal: Occupant Behaviour-Centric Building Design and Operation, 2018.

[21] P.B. Franceschini, L.O. Neves, A critical review on occupant behaviour modelling for building performance simulation of naturally ventilated school buildings and potential changes due to the COVID-19 pandemic, Energy Build. 258 (2022), 111831, https://doi.org/10.1016/j.enbuild.2022.111831.

[22] W. O'Brien, A. Wagner, M. Schweiker, A. Mahdavi, J. Day, M.B. Kjærgaard, S. Carlucci, B. Dong, F. Tahmasebi, D. Yan, T. Hong, H.B. Gunay, Z. Nagy, C. Miller, C. Berger, Introducing IEA EBC annex 79: key challenges and opportunities in the field of occupant-centric building design and operation, Build. Environ. 178 (February) (2020), https://doi.org/10.1016/j.buildenv.2020.106738.

[23] J. Donges, A. Prada, F. Cappelletti, A. Gasparella, The role of occupant behavior models in multi-objective optimization analysis, in: Proceedings of 6th International High Performance Buildings Conference at Purdue, vols. 1–10, 2021. West Lafayette (Indiana), U.S., 24th-28th May 2021.

[24] R. Albertin, Contagion Risk Assessment for COVID-19 Variants with A Dynamic Approach for A Multizone Building Model, Of University Classrooms, 2022.

[25] X. Shi, B. Si, J. Zhao, Z. Tian, C. Wang, X. Jin, Magnitude , Causes , and Solutions of the Performance Gap of Buildings : A Review, vols. 1–21, 2019, https://doi.org/10.3390/su11030937.

[26] Se-Hoon Hyun, Cheol-Soo Park, Godfried Augenbroe, Uncertainty and sensitivity analysis of natural ventilation in high-rise apartment buildings, Proceedings: Build. Simulat. (2007) 1013–1020.

[27] F. Haldi, A probabilistic model to predict building occupants' diversity towards their interactions with the building envelope, in: 2013: 13th Conference of the International Building Performance Simulation Association, Proceedings of BS, 2013, pp. 1475–1482. August 2013.

[28] F. Morandi, J. Donges, I. Pittana, A. Prada, F. Cappelletti, A. Gasparella, Modelling occupan ts ' behaviour to improve the building performance simulation of classrooms, in: Proceedings of 5th Building Simulation Applications Conference BSA 2022, 2022. Bolzano, Italy, 29*th June-1st July 2022*.

[29] CEN, European Committee for Standardization, UNI EN 16798-7 Energy Performance of buildings - Ventilation for buildings - Part 7: Calculation methods for the determination of air flow rates in buildings including infiltration (Modules M5-5), 2018, pp. 33–35. Bruxelles, 2018.

[30] D.A. Coley, Representing top-hung windows in thermal models, Int. J. Vent. 7 (2) (2008) 151–158, https://doi.org/10.1080/14733315.2008.11683807.

[31] L. Maciel, M. Oliveira, S. Barbosa, J. Carlo, Á. Tibiriçá, Influence of Application of Accurate Airflow Resistance on Openings with Different Configurations of Shading Devices on the Building Thermal Performance, 2017.

[32] R. Andersen, V. Fabi, J. Toftum, S.P. Corgnati, B.W. Olesen, Window opening behaviour modelled from measurements in Danish dwellings, Build. Environ. 69 (2013) 101–113, https://doi.org/10.1016/j.buildenv.2013.07.005.

[33] F. Haldi, D. Robinson, Interactions with window openings by office occupants, Build. Environ. 44 (12) (2009) 2378–2395, https://doi.org/10.1016/j.buildenv.2009.03.025.

[34] M. Quante, E. Kaplan, M. Rueschman, M. Cailler, O. Buxton, S. Redline, Practical considerations in using accelerometers to assess physical activity, sedentary behavior, and sleep, Sleep Health 1 (Issue 4) (2015) 275–284, https://doi.org/10.1016/j.sleh.2015.09.002. ISSN 2352-7218.

[35] F. Stazi, F. Naspi, G. Ulpiani, C. Di Perna, Indoor air quality and thermal comfort optimization in classrooms developing an automatic system for windows opening and closing, Energy Build. 139 (2017) 732–746, https://doi.org/10.1016/J.ENBUILD.2017.01.017.

[36] B.K. Clark, E.A. Winkler, C.L. Brakenridge, S.G. Trost, G.N. Healy, in: Using Bluetooth Proximity Sensing to Determine where Office Workers Spend Time at Work, 2018, https://doi.org/10.1371/journal.pone.0193971.

[37] C. Medina, J.C. Segura, Á. De la Torre, Ultrasound indoor positioning system based on a low-power wireless sensor network providing sub-centimeter accuracy, Sensors (Switzerland) 13 (3) (2013) 3501–3526, https://doi.org/10.3390/s130303501.

[38] M. Faltýnová, E. Matoušková, J. Šedina, K. Pavelka, Building facade documentation using laser scanning and photogrammetry and data implementation into BIM, Int. Arch. Photogrammetr. Remote Sens. Spat. Inform. Sci. - ISPRS Arch. 41 (July) (2016) 215–220, https://doi.org/10.5194/isprsarchives-XLI-B3-215-2016.

[39] J. Donges, F. Morandi, A. Prada, F. Cappelletti, A. Gasparella, Development of a camera-based tool to monitor non-binary occupants ' interaction with windows and shadings, in: Proceedings of 7th International High Performance Buildings Conference at Purdue, West Lafayette (Indiana), U.S., 2022, 10th-14th July 2022.

[40] N. Alishahi, M.M. Ouf, M. Nik-Bakht, Using WiFi connection counts and camera-based occupancy counts to estimate and predict building occupancy, Energy Build. 257 (2022), 111759, https://doi.org/10.1016/j.enbuild.2021.111759.

[41] B. Pavlin, G. Pernigotto, F. Cappelletti, P. Bison, R. Vidoni, A. Gasparella, Real-time monitoring of occupants' thermal comfort through infrared imaging: a preliminary study, Buildings 7 (1) (2017).

[42] M. Kim, I. Konstantzos, A. Tzempelikos, Real-time daylight glare control using a low-cost, window-mounted HDRI sensor, Build. Environ. 177 (January) (2020), 106912, https://doi.org/10.1016/j.buildenv.2020.106912.
[43] M. Kim, A. Tzempelikos, Performance evaluation of non-intrusive luminance mapping towards human-centered daylighting control, Build. Environ. 213 (January) (2022), 108857, https://doi.org/10.1016/j.buildenv.2022.108857.
[44] F. De Oliveira, S. Moreau, C. Gehin, A. Dittmar, Infrared imaging analysis for thermal comfort assessment, Ann. Int. Conf. IEEE Eng. Med. Biol. - Proc. 17 (2007) 3373–3376, https://doi.org/10.1109/IEMBS.2007.4353054.
[45] P.W. Tien, S. Wei, J.K. Calautit, J. Darkwa, C. Wood, Real-time monitoring of occupancy activities and window opening within buildings using an integrated deep learning-based approach for reducing energy demand, Appl. Energy 308 (December 2021) (2022), 118336, https://doi.org/10.1016/j.apenergy.2021.118336.
[46] J. Wong, J. Donges, A. Gasparella, A. Rysanek, A training dataset for machine learning-based prediction of window opening position in a naturally ventilated building, in: E3S Web of Conferences, vol. 396, EDP Sciences, 2023, 02034.
[47] D. Luong, R. Richman, M. Touchie, Towards window state detection using image processing in residential and office building facades, Build. Environ. 207 (PB) (2022), 108486, https://doi.org/10.1016/j.buildenv.2021.108486.
[48] P. Müller, G. Zeng, P. Wonka, L. Van Gool, Image-based procedural modeling of facades, in: Proceedings of the ACM SIGGRAPH Conference on Computer Graphics, 2007, https://doi.org/10.1145/1275808.1276484. July.
[49] C. Sun, X. Guo, T. Zhao, Y. Han, Real-time detection method of window opening behavior using deep learning-based image recognition in severe cold regions, Energy Build. 268 (2022), 112196, https://doi.org/10.1016/j.enbuild.2022.112196.
[50] K.W. Kim, H.G. Hong, G.P. Nam, K.R. Park, A study of deep CNN-based classification of open and closed eyes using a visible light camera sensor, Sensors (Switzerland) 17 (7) (2017), https://doi.org/10.3390/s17071534.
[51] C.P. Papageorgiou, M. Oren, T. Poggio, A general framework for object detection constantine, in: Computer Vision, 1998, Sixth International Conference On, 1998, pp. 555–562, 0(January, http://www.computer.org/portal/web/csdl/doi/10.1109/ICCV.1998.710772.
[52] Rafael C. Gonzalez, Digital Image Processing, fourth ed., Pearson, Harlow, 2018. Print.
[53] A. Medellin, The New Raspberry Pi Camera Is a Worthwhile Upgrade, 2020. https://www.premiumbeat.com/blog/new-raspberry-camera-upgrade/.
[54] H.D. Cheng, X.H. Jiang, Y. Sun, Jingli Wang, Color image segmentation: advances and prospects, Pattern Recogn. 34 (Issue 12) (2001) 2259–2281, https://doi.org/10.1016/S0031-3203(00)00149-7. ISSN 0031-3203.
[55] Valín Fernández, J.V. Alberto, Mastering OpenCV 4 with Python : a practical guide covering topics from image processing, in: Augmented Reality to Deep Learning with OpenCV 4 and Python 3. 7, Web, 2019.
[56] C. Hughes, P. Denny, E. Jones, M. Glavin, Accuracy of fish-eye lens models, Appl. Opt. 49 (17) (2010) 3338–3347, https://doi.org/10.1364/AO.49.003338.